Research
Synthetic Biology—Article

An Additive Manufacturing Approach that Enables the Field Deployment of Synthetic Biosensors

Daniel Wolozny [a], John R. Lake [b], Paul G. Movizzo [b], Zhicheng Long [b,*], Warren C. Ruder [b,*]

[a] Department of Biological Systems Engineering, Virginia Polytechnic Institute and State University, Blacksburg, VA 24061, USA
[b] Department of Bioengineering, University of Pittsburgh, Pittsburgh, PA 15219, USA

A B S T R A C T

The tools of synthetic biology can be used to engineer living biosensors that report the presence of analytes. Although these engineered cellular biosensors have many potential applications for deployment outside of the lab, they are genetically modified organisms (GMOs) and are often considered dangerous. Mitigating the risk of releasing GMOs into the environment while enabling their use outside a laboratory is critical. Here, we describe the development of a biosensing system consisting of a synthetic biological circuit, which is engineered in *Escherichia coli* that are contained within a unique 3D-printed device housing. These GMOs detect the chemical quorum signal of *Pseudomonas aeruginosa*, an opportunistic pathogen. Using this device, the living biosensor makes contact with a specimen of interest without ever being exposed to the environment. Cells can be visually analyzed in the field within culture tubes, or returned to the lab for further analysis. Many biosensors lack the versatility required for deployment in the field, where many diseases can go undiagnosed due to a lack of resources and equipment. Our bioassay device utilizes 3D printing to create a portable, modular, and inexpensive device for the field deployment of living biosensors.

© 2019 THE AUTHORS. Published by Elsevier LTD on behalf of Chinese Academy of Engineering and Higher Education Press Limited Company. This is an open access article under the CC BY-NC-ND license (http://creativecommons.org/licenses/by-nc-nd/4.0/).

1. Introduction

Synthetic biology is a combination of biology and engineering that attempts to gain new understanding and utilization of the natural world by applying engineering principles to design genetic elements for cellular control. Common examples of synthetic biology include memory switch [1] and oscillator [2] circuits that enable cells to switch between distinct states based on chemical or other input. This ability to sense an input from the environment enables cells to serve as a biosensor. A synthetically engineered biosensor [3–6] takes advantage of the versatility of living cells to detect and process inputs into analyzable outputs. Living cells, especially bacteria, can survive under many conditions [7,8] and can be engineered to detect and diagnose infectious biomarkers in clinical settings.

Genetically modified organisms (GMOs) are regulated by many laws and governmental bodies [9–13], making them difficult to deploy outside of laboratory settings. To allow engineered

biosensors to be deployed for disease diagnosis in the field, these regulations must be satisfied. Additive manufacturing, in the form of three-dimensional (3D) printing, can serve as a solution to isolate GMOs from the environment when used in the field.

Critical additive manufacturing approaches were first commercialized three decades ago [14]. Since then, additive manufacturing technology has evolved rapidly, making 3D printers widely available. The 3D printers utilized for this work function by successively depositing layers of extruded filaments to build a 3D structure [15]. These types of 3D printers have already been proven to successfully design, print, and test medically relevant devices [16,17].

In this work, we chose to employ a robust approach for detecting the quorum signal of *Pseudomonas aeruginosa* (*P. aeruginosa*) that is frequently used in synthetic biology (Fig. 1(a)). The living biosensor consists of engineered *Escherichia coli* (*E. coli*) that are designed to detect the presence of this quorum signal, *N*-3-oxododecanoyl homoserine lactone (3O-C12). The living biosensor was constructed by introducing components of *P. aeruginosa*'s native 3O-C12 signaling pathway to *E. coli*. Here, a transcription factor, LasR, acts as a signal transducer by binding 3O-C12 and dimerizing. This complex then binds to a transcription activation domain found within its cognate promoter, PLas [6,18,19], which
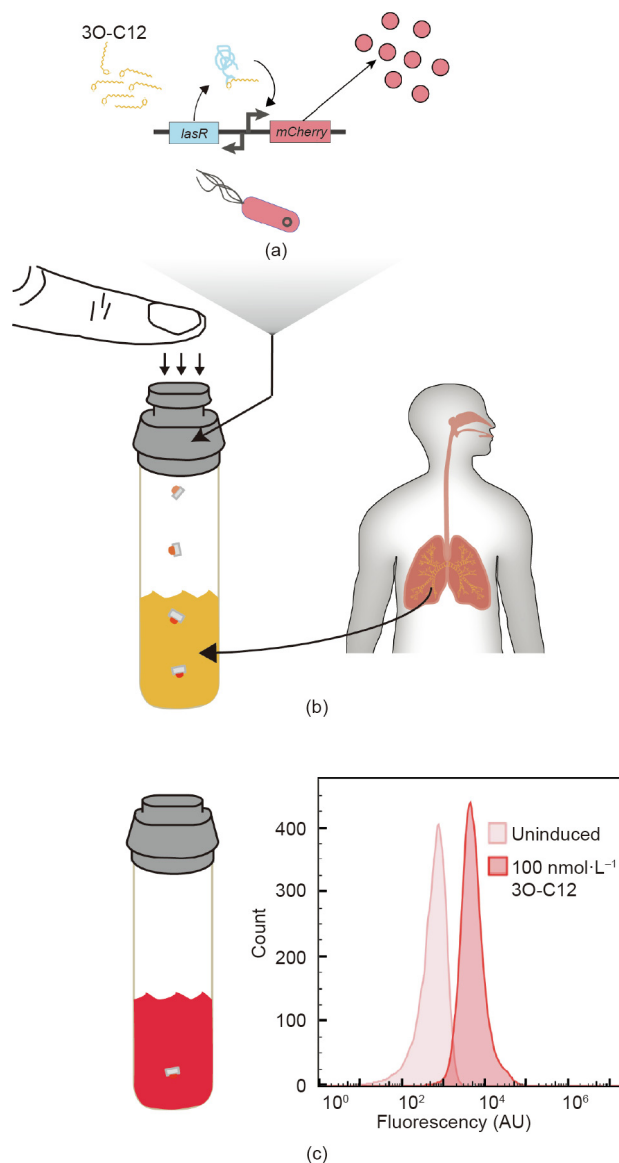
Fig. 1. Field detection of 3O-C12 through the use of a GMO and a 3D-printed enclosure. (a) The 3O-C12 biosensor was engineered to constitutively express a protein, LasR, which is able to bind a 3O-C12 molecule. Once bound to 3O-C12, the LasR protein dimerizes and binds to a DNA region contained in the PLas promoter, which promotes the expression of mCherry. (b) The biosensor is placed in a 3D-printed enclosure. A biological sample can then be extracted and placed in a sample tube that is connected to the 3D-printed device. The device cover is then pressed, causing the biosensor to fall into the sample. (c) The biosensor turns red to report exposure to 3O-C12 in the sample; this signal can then be quantified using flow cytometry. Histograms represent data collected for 10 000 events for both the un-induced and the 100 nmol·L^{-1} 3O-C12 samples (three samples).

is also transplanted into *E. coli*. In our design, once bound, LasR promotes the expression of the gene for mCherry, a red fluorescent protein. We specifically chose 3O-C12 as the chemical to be detected due to its relevance in medical settings [20–25].

As an example of the clinical relevance of this approach, in rural and less-developed areas, lung infections from the organism *P. aeruginosa* can be acquired in local clinics. Upon lung infection by *P. aeruginosa* (Fig. 1(b)), the organism may be found in lung sputum samples. This sputum can be collected and placed within commercially available sample tubes. As a result, an approach enabling these samples to be immediately analyzed in the field, using the tools of synthetic biology, would be ideal for early diagnosis.

In the solution presented here, the sample tube is mated with a unique cap containing the synthetic biological sensor (Fig. 1(b)). This unique 3D-printed device completely encases the living biosensor, allowing its transport from the laboratory, while also allowing the sensor to be introduced directly to a sample. When the sputum sample is ready to be analyzed, force is applied to the device by the user's finger, causing the bacterial biosensor to break out of the housing and fall into the sample. Detection of 3O-C12, which will be produced by *P. aeruginosa* in the sample or is already present in the sample, causes the living biosensor to produce mCherry (Fig. 1(c)) and turns the sample red; this color can be detected through fluorescence analysis or visually with the human eye. Thus, a colorimetric change in the sample can indicate the presence of *P. aeruginosa* in the lungs.

P. aeruginosa functions as an opportunistic pathogen in patients with cystic fibrosis, causing recurring infections of the lungs and respiratory tract. Current diagnostic technology typically takes the form of enzyme-linked immunosorbent assays (ELISAs) [26] and real-time polymerase chain reaction (PCR) assays [27], which are either expensive or require extensive training to administer. The sensing approach described here could serve as a simple and inexpensive complement to current diagnosis techniques for detecting *P. aeruginosa*. Since the cellular biosensor can be grown within a secure, 3D-printed device for containment, this device can be used as a platform for the deployment of synthetically engineered biosensors in the field.

2. Material and methods

2.1. Cell culture and molecular cloning

The *E. coli* strains used in this study were derived from the *E. coli* K12 parent strain and are listed in Table 1 [28]. *E. coli* cells were grown in batch culture at 37 °C in lysogeny broth (LB, Thermo Fisher Scientific Inc., USA) media [29]. Resistant transformants were selected using 100 μg·mL^{-1} kanamycin (Thermo Fisher Scientific Inc., USA). For cloning, NEB® Turbo Competent *E. coli* (New England Biolabs® Inc., USA) was used as the host to propagate the plasmids. Cells were grown at 37 °C in LB media supplemented with kanamycin. For growth on plates, LB media was supplemented with 2% agar (w/v) and kanamycin.

The plasmids used in this study are listed in Table 1 and were constructed through standard molecular cloning approaches [29,30]. The sensor plasmid was constructed by first amplifying an 843 bp PLtetO-1–*lasR* DNA region from a plasmid, pKDT17, which was ordered from Addgene.org, and originally came from the laboratory of Dr. Peter Greenberg. A 711 bp *mCherry* gene was amplified to produce an RBS–*mCherry*–t0 fragment, which was inserted into pKDT17 to obtain the LasR sensor plasmid, pDW065 (Fig. 2).

2.2. Dose–response characterization

To study this gene network's dose response, starter cultures of *E. coli* with pDW065 were grown overnight in LB media supplemented with 50 μg·mL^{-1} kanamycin. The cultures were diluted

Table 1
List of plasmids, strains, relevant characteristics, and origins.

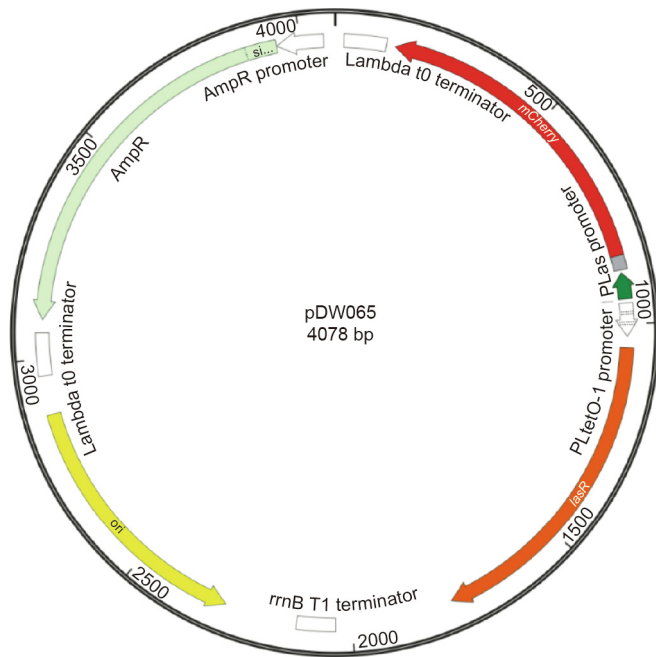| Name	Mutations	Origin
NEB Turbo®	*E. coli* K12 wild type	New England Biolabs® Inc.
MG1655 WT	*E. coli* K12 wild type	*E. Coli* Genetic Stock Center
pWR011	PLtetO-1–*mCherry*	Ruder Lab
pKDT17	*lasR*, *lasB*::*lacZ*	Pearson et al. [28]
pDW065a	PLtetO-1–*lasR*, PLtetO-1–*mCherry*	This study
pDW065	PLtetO-1–*lasR*, PLas–*mCherry*	This study

Fig. 2. 3O-C12 sensor plasmid map. The 3O-C12 sensor, also known as pDW065, is composed of three main elements: the plasmid backbone, the *lasR* cassette, and the *mCherry* cassette. The backbone consists of an ampicillin-resistance cassette and a pUC origin of replication. The *lasR* gene is placed under the control of a PLtetO-1 promoter, while the *mCherry* gene is under the control of the PLas promoter, which contains a binding site for the LasR protein.

to 0.2 OD$_{600}$ (i.e., an optical density measured at 600 nm) and allowed to grow until reaching 0.6 OD$_{600}$. The cultures were then diluted again, supplemented with 0–100 µmol·L^{-1} 3O-C12 (Sigma-Aldrich Corporation, USA), and maintained at the exponential phase at 37 °C until fully induced (about 8 h). Cultures at 0.6 OD$_{600}$ were diluted to 1:100 in filtered phosphate-buffered saline (PBS, Thermo Fisher Scientific Inc., USA) and fluorescence was measured using an Accuri™ C6 flow cytometer (Becton, Dickinson and Company, USA).

2.3. Design and fabrication of acrylonitrile butadiene styrene devices

The 3D-printed device was designed using Autodesk Inventor® (Autodesk Inc., USA), where it was rendered into a 3D model. The designed model was then exported as an STL file, which is a file format that can be used by Z-suite® (Zortrax Company, Poland), the software that was used to translate the 3D object into a set of printer instructions. The Z-suite® software was then used to export the file as a z-code file, which was used in a Zortrax M200 (Zortrax Company, Poland) to print the 3D design using an acrylonitrile butadiene styrene (ABS) variant, ABS ULTRAT. This proprietary ABS variant is composed of ABS (90%–100%), stabilizer (0%–5%), lubricants (0%–2%), mineral oil (0%–4%), tallow (0%–4%), wax (0%–4%), polycarbonate (PC, 0%–3%) and anti-oxidant (< 2%).

2.4. Device surface polishing

In order to smooth the surface roughness of the device components post-printing, the 3D-printed components were first placed on a sterile surface. Paper towels were attached to the inner surface of a 1000 mL beaker and saturated with acetone. The beaker was inverted over the device components, and care was taken to avoid direct contact between the liquid acetone and the components. After 1 h, the beaker was removed and the devices were exposed to ambient air for 2 h.

2.5. Device use and operation

To encase the 3O-C12 living biosensor into the 3D-printed device, a 40 µL agar plug was added to the bacterial well in the housing; the engineered *E. coli* cells were then plated onto the agar surface. After overnight culture, the plunger was pressed into the housing and a press-fit seal was formed to isolate the bacterial cells from the environment. The cap containing the living biosensor could then be safely transferred to the field and stored in a refrigerator for up to 30 d before use. When ready for use, the sample to be examined was placed into a 14 mL culture tube. The culture tube cap was removed and the assembled device containing the living biosensor was then snapped into place onto the culture tube. To activate the biosensing, the cover was firmly pressed with a lateral pinch grip until the bacterial well fell into the culture tube. The cell culture was then incubated at 37 °C for 8–9 h and subsequently detected with fluorescence spectroscopy, or simply with the human eye. For the flow cytometry analysis used in this study, samples were collected at an OD$_{600}$ of 0.6 and diluted to 1:100 in deionized water. Fluorescence measurements were acquired using an Accuri™ C6 flow cytometer. Following the completion of experiments, the system can be sterilized in an autoclave; or, if an autoclave is not available, the components can be disassembled and immersed in sodium hypochlorite (i.e., bleach).

2.6. Gene regulatory network modeling

We engineered an *E. coli* biosensor capable of expressing mCherry when exposed to 3O-C12. The activator, LasR, was constitutively produced in an inactive state. When 3O-C12 is introduced to the cell, it binds to LasR. This complex activates a gene regulatory network. As we did not engineer any post-transcriptional regulation, the general behavior of the regulatory gene networks can be modeled by the dynamics of the transcriptional response site.

To capture the underlying dynamics of our system, we decided to employ the Michaelis–Menten formalism for the modeling transcription. As we used a high copy count plasmid, we can assume that stochastic effects are negligible for specific genetic components. This allows us to simplify our simulation with a set of ordinary differential equations.

By assuming that the inducer, 3O-C12, is well mixed within our reaction chamber and that transport of 3O-C12 into the cytosol is consistent among individual cells, we can model the transcriptional response to 3O-C12 as shown in Eq. (1). Note that this equation assumes that the majority of post-transcriptional events (translation and protein maturation) occur consistently and linearly in response to mRNA production. This is a fair assumption, if we also assume that the ribosome binding site strengths are constant and that there is an abundance of resources and ribosomes within the cell.

$$\frac{d[\text{mCherry}_i]}{dt} = V_{1\text{max}} \frac{[\text{3O-C12}]^n}{K_1^n + [\text{3O-C12}]^n} + V_{1\text{leak}} - d_1[\text{mCherry}_i] \qquad (1)$$

Eq. (1) relates the time rate of change of mCherry to a number of inputs and parameters that drive transcriptional events.

Inherent in this model is the assumption that LasR concentrations within the cells remain relatively constant. The first term on the right side of Eq. (1) is a Hill function [31] relating the intracellular concentration of 3O-C12, [3O-C12], to the rate of mCherry production. This term is a function of the concentration of arabinose but it includes parameters for the maximum transcription rate, $V_{1\text{max}}$, and the kinetic coefficient, K_1. In addition, the Hill coefficient, n, relates the degree of cooperativeness of the RNA polymerase binding to the promoter site.

The second term on the right side of Eq. (1), V_{1leak}, describes the "leak" of the promoter site. In physical terms, this is the rate of mCherry produced in the absence of 3O-C12. The final term on the right side describes the rate of degradation of mCherry within the cell. This term relates a decay constant, d_1, to the concentration of mCherry, $[mCherry_i]$. This equation may be fit to experimental data in order to better predict and model underlying dynamics.

2.7. Model derivation: doseresponse curve fitting, simulation, and plotting

Experimental data were analyzed and fit according to Eq. (1) using the MATLAB® (MathWorks Inc., USA) optimization toolbox. Once parameter values were identified, fits were confirmed with the MATLAB curve-fitting toolbox. The goodness of fit for the simulated equations was evaluated using the R^2 value. Simulations were coded in Python and numerically integrated using LSODE [32] in the FORTRAN library. Simulations, with experimental data, were plotted in Python using the Matplotlib library.

2.8. Model derivation: finite element analysis of biosensor

Finite element analysis was performed using COMSOL (COMSOL Multiphysics® v5.2, COMSOL Inc., Sweden). All simulation results represent a stationary study performed using the Solid Mechanics module. Autodesk Inventor solid model files were imported into COMSOL to define the geometry for these simulations. Material properties were then entered into COMSOL to define the properties of our ABS material for analysis. Boundary constraints and applied loads were then defined. All simulation plots shown here were generated using COMSOL's integrated graphics.

3. Results

The 3D-printed device was designed to attach to a common laboratory sample tube form factor (Fig. 3(a)) to ensure ease of

use. The device consists of two components (Fig. 3(b)), referred to herein as the "housing" and "cover." The cover serves to isolate the contents enclosed in the housing interior from the surrounding environment. In addition, the top of the cover is designed to be ergonomic for pressing with a thumb or forefinger. Once assembled, the device can be enclosed within a rectangular prism with dimensions of approximately 0.026 m × 0.026 m × 0.023 m. A cross-sectional schematic of the assembled device (Fig. 3(c)) shows the housing and cover held together by a press-fit. The housing holds a bacterial well, which contains rich agar with a small lawn of bacteria; this serves to sustain and contain the bacterial biosensor within the device. Next, we added small mechanical features to the device, the design of which was based on modeling with a finite element method software suite [33], COMSOL Multiphysics®. It is important to note that our models were based on construction with ABS, a thermoplastic. Thermoplastic polymers become pliable after heating, harden upon cooling, and are frequently used in 3D printing. ABS is often used because its glass transition temperature of 105 °C makes it well-suited for 3D printing, as the extruder temperature in many 3D printers is set at 230 °C [34]. This high printing temperature also enhances the sterility of the printed device.

In addition to the cover, housing, and bacterial well features discussed above, we designed a small mechanical feature that enables an axial force (i.e., a force applied directly downward on the cover, along the major axis of the sample tube) to cause the bottom of the housing to quickly separate from the housing, thus releasing the biosensor into the sample during a (designed) catastrophic failure. In order to cause this fast yielding, we created two depressed annuli features in the housing bottom (on both the interior and exterior, shown in Figs. 4 and 5 with additional detail). Herein, we refer to these annuli as "stress-focusing cutouts." These cutout features serve to concentrate the stresses that develop from applied axial force on the cover, thus allowing simple activation of the device by means of a user's thumb using a pinch grip.

Finite element analysis was used to numerically evaluate the stresses that developed within the device when force was applied
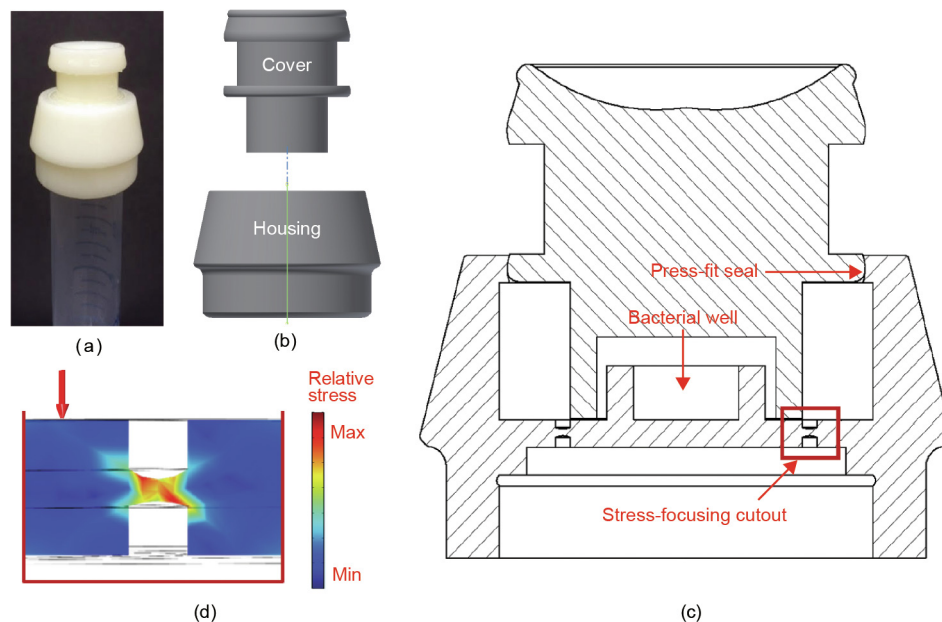

Fig. 3. Device details and schematic. (a) The 3D-printed device can be attached to a test tube, where it forms a seal. This device is separated into two parts: the cover and the housing. (b) The device cover is sealed onto the housing using a press-fit. (c) The device housing contains a bacterial culture well, which serves as a chamber in which culture nutrients, agar, and living biosensors can be deposited. The housing is designed with a stress-focusing cutout, which serves to concentrate the pressing force transmitted from the cover to separate the bacterial well from the housing. (d) The stresses concentrated by the stress-focusing cutout were modeled using COMSOL to ensure that the device is usable with a one-handed lateral pinch grip. Max: maximum; min: minimum.
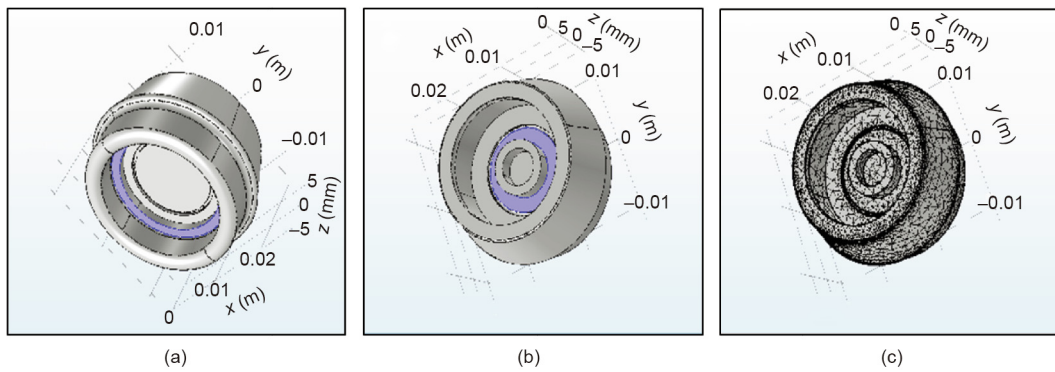
Fig. 4. Device boundary constraints, loads, and mesh elements for stress simulation. (a) Boundary constraints. The purple highlighted boundary of the biosensor housing is the sole fixed boundary constraint used for all simulations. All other boundaries are free. (b) Boundary loads. The purple highlighted boundary shows the surface where the sensor-activating lid applies a distributed pressure load during use. All simulations used a total load of 100 N distributed across this highlighted area. (c) Mesh elements. COMSOL predefined "normal" meshing was used for all simulations.
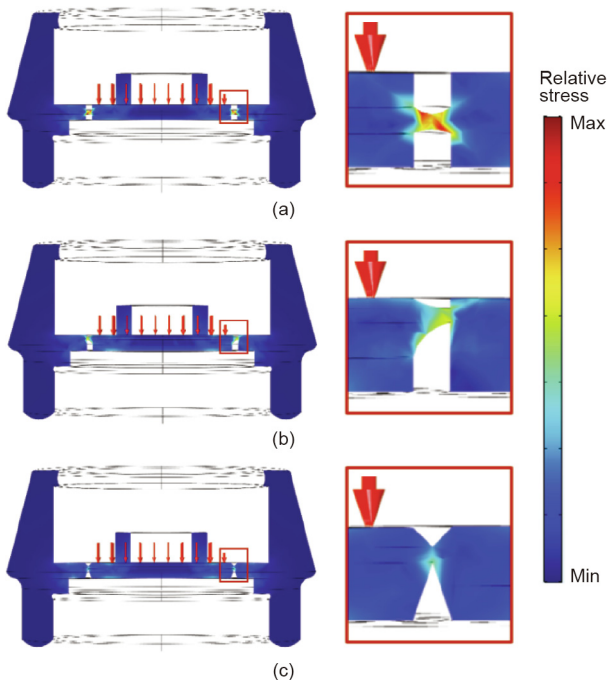

Fig. 5. Cross-sections of three different device iterations with von Mises stress distribution. (a) Final design configuration and stress distribution of the stress-focusing cutout portion of the biosensor housing; (b) an alternative design with arcs coming to a point; (c) an alternative design with peaks. The largest stress and best distribution of high stress, as shown here, resulted in the final design in (a) being chosen. All simulations had the following material properties: a material density of 1150 kg·m^{-3}, Young's modulus of 2 GPa, and Poisson's ratio of 0.35. All simulations used a total load of 100 N distributed across the boundary load area. COMSOL predefined "normal" meshing was used for all simulations.

during its use. The stress profile through the stress-focusing cutout was modeled using COMSOL for different designs in order to arrive at the final version, which is presented in this paper [33]. An evenly distributed pressure load was applied to the surface of the housing by the cover to generate stress in the cutout. Three different designs of the stress-focusing cutout were modeled in order to identify the stress magnitude and concentration in the cutout for a given applied force. Relative to other preliminary designs, the final design presented here (Fig. 3(d)) has both the highest maximum stress developed within the cutout for a given applied force and the best spatial distribution of the high stress concentration through the cutout. This design of the cutout allows our device

to be constructed from a relatively high-strength material, while still requiring a relatively small force to activate the sensor by breaking the cutout.

The device was also designed to be simple to assemble and use, as shown in Fig. 6. A 40 μL agar plug was added to the bacterial well and the 3O-C12 living biosensor was plated on its surface. The device cover was then fit onto the housing and attached to a culture tube, which isolates the biological sample from the environment. The user's thumb is then used to activate the device. This applied force on the cover develops stress in the stress-focusing cutout within the housing. The bacterial well then breaks away from the housing and falls into the sample. After analysis, the cover can be pushed into the housing to create the second stage of the press-fit seal, thus preventing the sample within the test tube from escaping during a leak, in the event that the device is inverted or agitated. This seal also allows the user to transfer the biohazardous waste back to a biosafety lab for proper disposal.

Upon immersion in the sample, the biosensor was grown for 8 h. The 3O-C12-activated biosensor then produced mCherry protein. As shown in the flow cytometry analysis (Fig. 7(a)), the induced biosensor showed a shift in fluorescence emitted at 590 nm, which was distinctly separate from the un-induced biosensor control fluorescent peak. In our dose–response experiment (Fig. 7(b)), 0.1 μmol·L^{-1} of 3O-C12 was sufficient to induce the living biosensor to produce visible fluorescence in the tube after 8 h growth. When quantified with a flow cytometer, the dynamic range of the sensor was observed to be in the range of 0.01–1 μmol·L^{-1} 3O-C12.

4. Discussion

Although synthetic biology-based biosensors can be versatile in the detection of chemical inputs, many are currently confined to a laboratory setting due to regulations that restrict the use and transport of GMOs. It is worth noting that a paper-based synthetic biosensor was recently developed by Pardee et al. [35]. This paper-based biosensor was developed by freeze-drying cell-free synthetic gene networks on paper to create materials that had the fundamental transcription and translation properties of a cell yet remained abiotic. The paper-based approach offers faster detection than cell-based living biosensors and eliminates the use of living bacterial cells for detection, which makes it suitable for the safe deployment of engineered gene circuits beyond the lab. However, the paper-based biosensor requires different sample processing and a different set of specialized materials. Thus, the system we describe here allows the complementary
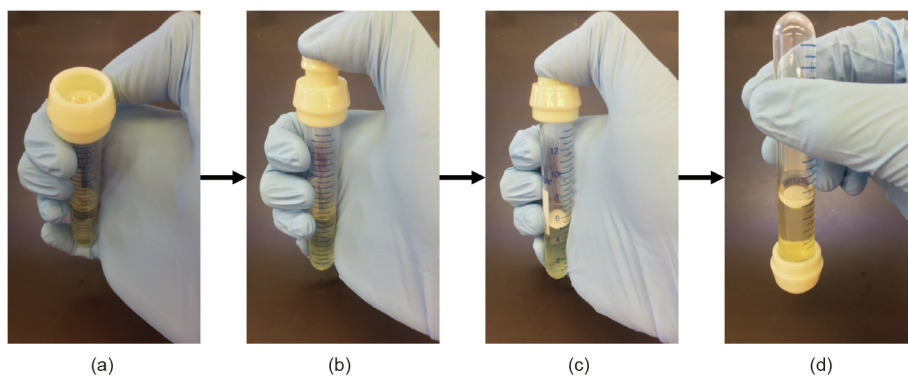
Fig. 6. Demonstration of device use. (a) Agar is added to the bacterial well within the bioassay device. (b) The device lid is aligned with the device base and pressed with the thumb until the press-fit seals. Using the thumb, force can be applied to the lid, which releases the press-fit and directs force onto the stress-focusing cutout. (c) The bacterial well then falls into the sample, where it inoculates the sample with the biosensor. (d) The liquid and bacteria within the test tube remain isolated from the environment.
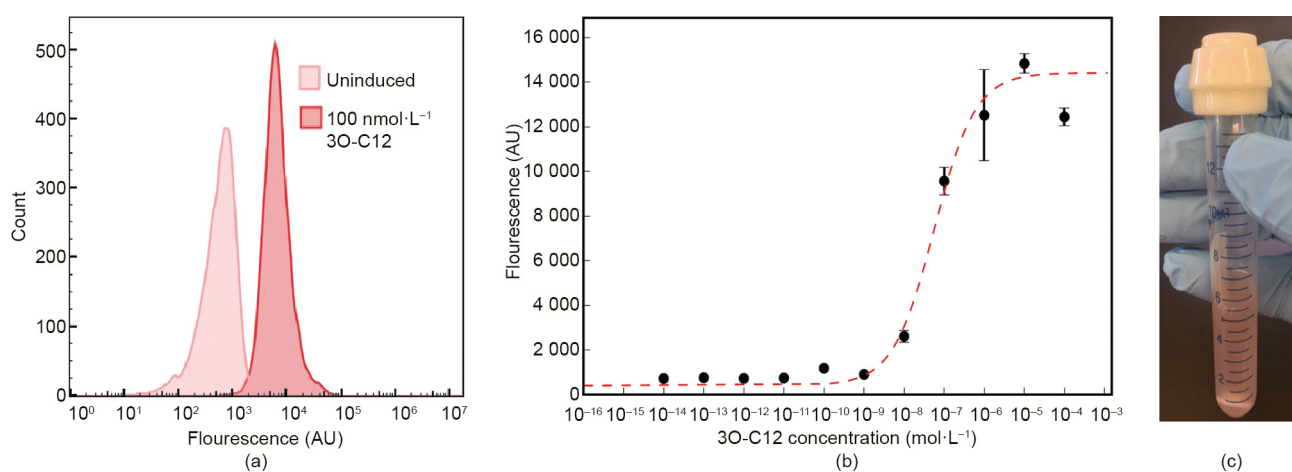

Fig. 7. Biosensor dose–response curve. (a) When induced with 3O-C12, the biosensor goes from an un-induced state to an induced state. After being induced, the biosensor fluoresces by producing mCherry protein. The biosensor was exposed to varying concentration decades of 3O-C12 and maintained in exponential state. Data were collected for 10 000 events for the un-induced and the 100 nmol·L^{-1} 3O-C12 samples (three samples). (b) After 8 h of induction, the biosensor reaches an equilibrium state of mCherry expression, which can be quantified. The system can then be fitted to a Hill function with an R^2 value of 0.987. (c) With enough time, the sensor becomes a toggle switch and is able to output an on/off response.

use of living biosensors, which can potentially be integrated in parallel with cell-free detection methods in the future. We envision our system being especially beneficial in areas that lack significant medical infrastructure or access to healthcare.

The 3O-C12 biosensor is able to detect 3O-C12 concentrations ranging from 0.1 to 10 µmol·L^{-1}. It is well documented [36–39] that a *P. aeruginosa* infection in the respiratory tracts can cause tissue inflammation. Although the specific method of action of chemical 3O-C12 remains unknown, it is believed to occur through interactions with toll-like receptors on the cell's surface [40], which produce an inflammatory response. This inflammation is triggered by a 3O-C12 concentration in the range from 10 to 100 µmol·L^{-1}. The range of concentrations found in infected lungs lies outside of the dynamic response range of our 3O-C12 biosensor. However, a straightforward series of dilutions (e.g., 1/2, 1/4, . . .) with media—as is done for other quantification assays, such as the Bradford Assay [41]—can be performed before analysis. Diluting the sputum collected in media will also allow the cells to divide faster with a more suitable environment for growth.

The bioassay device can be fabricated anywhere a 3D printer is available. The 3D printer that we used for this research is sold for less than 2000 USD, and many new 3D printers can be purchased for prices ranging from 200 to 500 USD. Our bioassay device can also be fabricated quickly, as needed, with devices ready after less than 2 h (Fig. 8(a)). The material cost to manufacture one of the

3D-printed devices described here is approximately 0.50 USD, using 8 g of ABS. In comparison with the biosensor housing and cover, the biosensor itself contributes only a small portion of the overall cost of the device. The printer can be used at any location, making the deployment of this device flexible. Biosensors can also be readily grown, freeze-dried, and shipped worldwide. With a small quantity of freeze-dried biosensor loaded into the devices (Fig. 8(b)), they can be sealed and be ready for use. The devices can then be directly transported to the point-of-care for use (Fig. 8(c)). In the case of an accident, in which a device comes into contact with the environment, it is important to quantify how well the device isolates the biosensor from the environment. An experiment using nutrient-rich media (Fig. 8(d)) was used to simulate a worst-case scenario. When shaken at 140 r·min^{-1} in 100 mL of media (Fig. 8(e)), the bacterial well that had been introduced into the media was able to propagate cells immediately. When the entire intact device was submerged in media, the sealed device was able to isolate the biosensor from the environment for a period of 14 h before the cells escaped and showed visible turbidity in 100 mL of media.

In the field, a sputum sample (Fig. 9(a)) can be collected from the patient and diluted into a sample tube with cell media. To ensure that no bacteria outcompete the kanamycin-tolerant living biosensor in the sample, a kanamycin antibiotic could be added, making the bacterial samples from the patient's sputum unable
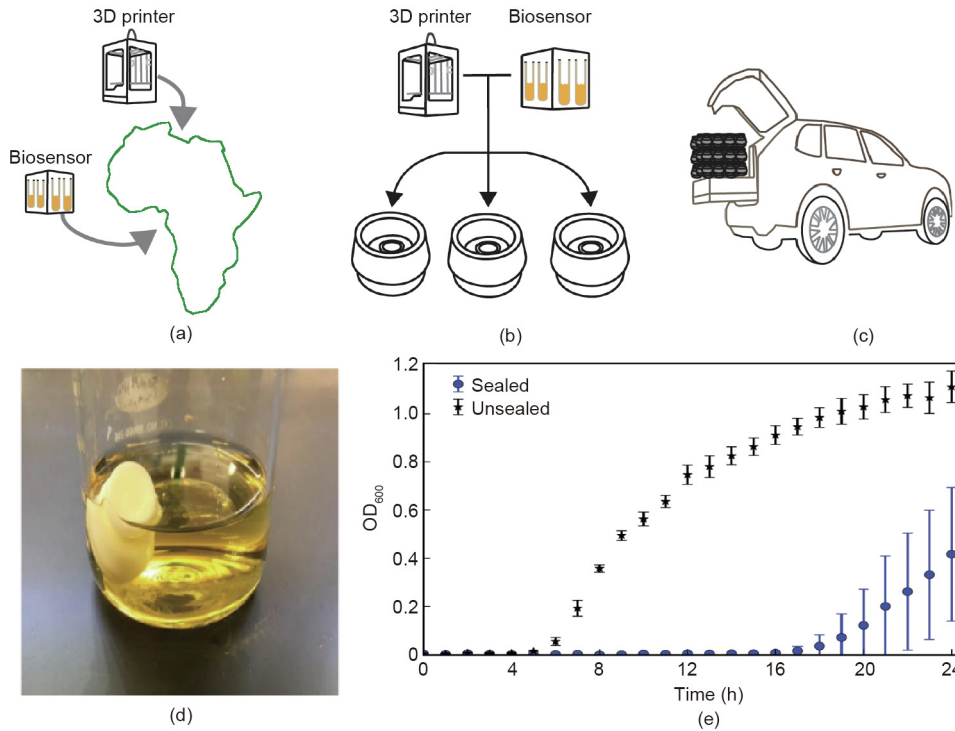
Fig. 8. From the printer, to the patient, to the lab. (a) A 3D printer is used to print the bioassay device. (b) The genetically engineered sensor is cultured within the 3D-printed bioassay device. (c) The device with the sensor is transported to the patient's location. (d) The device is water-resistant, so in the event that the device falls into a liquid, there is time to remove it without the escape of GMOs. (e) When the device is used normally, and the bacteria are directly deposited into nutrient-rich media, they will immediately begin to grow. However, the sealed device could also prevent liquid from reaching the cells for a period of 14 h in the event of device mishandling resulting in emersion in environmental liquids. Data collected for 10 000 events for the sealed and unsealed three samples.
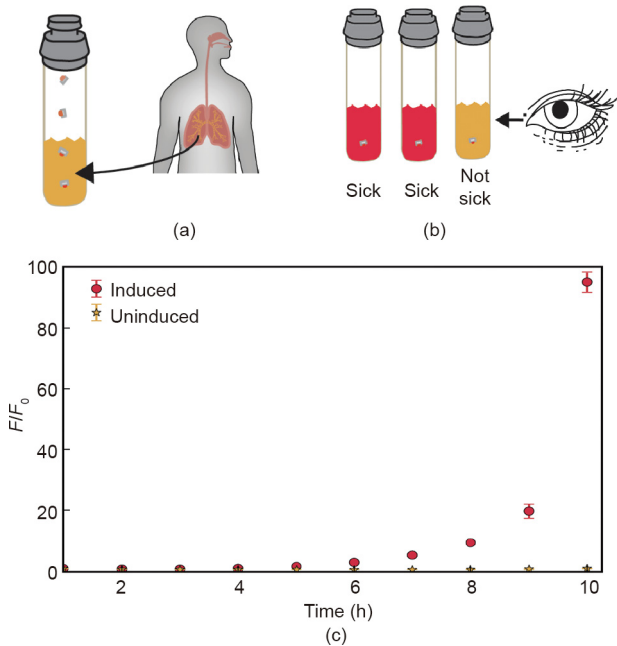

Fig. 9. Biosensor activity on contact with 3O-C12. (a) A sputum sample is taken from the patient and the 3D-printed device is collapsed to release the bacteria into the sample. (b) The biosensor is built to enable both quantification of 3O-C12 concentration and a more simple on/off behavior in which 3O-C12 at or above 10 nmol·L^{-1} will turn the sample visibly red. (c) The biosensor turns visibly red with a 98-fold fluorescence increase, compared with the initial fluorescence value, F/F_0, after 10 h of exposure to the inducer. mCherry protein production continues as long as cells remain exposed to the inducer. Data collected for 10 000 events for the un-induced and the 100 nmol·L^{-1} 3O-C12 samples (three samples).

to survive. The biosensor cover would then be pressed firmly and actuated, forcing the freeze-dried bacterial pellet to enter the sputum sample. Next, the tube could be incubated and analyzed in the field (Fig. 9(b)). The biosensor can simultaneously quantify specific levels of 3O-C12 exposure when maintained in exponential state or can switch into an on/off behavior by simply adding the biosensor to the sample (Fig. 9(c)). A 9 h incubation allows the biosensor to turn the liquid sample visibly red, thus serving as a two-state system that is useful to visually determine in the field whether a patient has a *P. aeruginosa* infection.

The device was designed to be fabricated and used by personnel or volunteers with minimal training. After attachment to a culture tube, the device and culture tube can be gripped by the hand, and the thumb can be used in a lateral pinch grip to activate the sensor. The average lateral pinch strength of an adult using the dominant hand ranges from approximately 5.0–7.5 kg of force [42], which is sufficient for the use of this device. Due to the design of the stress-focusing cutout presented here, the lateral pinch force generated by an adult will allow the device to reliably function in the field.

5. Conclusion

The experimental results presented here indicate that the 3O-C12 biosensor is able to sense inducer concentrations when *P. aeruginosa* biofilms are present, as in the case of recurring infections. The living biosensor, while useful for the purpose of detection, has the potential to face fewer regulatory hurdles due to its enclosure within the bioassay device, which permits its contained deployment outside the lab. The 3D-printed device turns the GMO into a component of the overall device and ensures that the biosensor is isolated from the environment. Thus, 3D printing this device enables our living biosensor, with its versatility to

process environmental input, to be field-deployed as a novel, cost-effective diagnostic technology.

Author contributions

Wolozny and Ruder conceived the idea for the system described here. All authors designed and performed the experiments, analyzed the data, discussed the results, wrote this manuscript and commented on the paper. Wolozny, Lake, Long, and Ruder revised the manuscript.

Compliance with ethics guidelines

Daniel Wolozny, John R. Lake, Paul G. Movizzo, Zhicheng Long, and Warren C. Ruder declare that they have no conflict of interest or financial conflicts to disclose.

References

[1] Gardner TS, Cantor CR, Collins JJ. Construction of a genetic toggle switch in *Escherichia coli*. Nature 2000;403(6767):339–42.
[2] Elowitz MB, Leibler S. A synthetic oscillatory network of transcriptional regulators. Nature 2000;403(6767):335–8.
[3] Balagaddé FK, Song H, Ozaki J, Collins CH, Barnet M, Arnold FH, et al. A synthetic *Escherichia coli* predator-prey ecosystem. Mol Syst Biol 2008;4 (1):187.
[4] Litcofsky KD, Afeyan RB, Krom RJ, Khalil AS, Collins JJ. Iterative plug-and-play methodology for constructing and modifying synthetic gene networks. Nat Methods 2012;9(11):1077–80.
[5] Brenner K, Karig DK, Weiss R, Arnold FH. Engineered bidirectional communication mediates a consensus in a microbial biofilm consortium. Proc Natl Acad Sci USA 2007;104(44):17300–4.
[6] Tamsir A, Tabor JJ, Voigt CA. Robust multicellular computing using genetically encoded NOR gates and chemical 'wires'. Nature 2011;469(7329):212–5.
[7] McDaniel LE, Bailey EG, Zimmerli A. Effect of oxygen-supply rates on growth of *Escherichia coli*. I. Studies in unbaffled and baffled shake flasks. Appl Microbiol 1965;13:109–14.
[8] Ratkowsky DA, Olley J, McMeekin TA, Ball A. Relationship between temperature and growth rate of bacterial cultures. J Bacteriol 1982;149 (1):1–5.
[9] Kuzma J, Besley JC. Ethics of risk analysis and regulatory review: from bio- to nanotechnology. NanoEthics 2008;2(2):149–62.
[10] Gregorowius D, Lindemann-Matthies P, Huppenbauer M. Ethical discourse on the use of genetically modified crops: a review of academic publications in the fields of ecology and environmental ethics. J Agric Environ Ethics 2012;25 (3):265–93.
[11] Kilama WL. Health research ethics in public health: trials and implementation of malaria mosquito control strategies. Acta Trop 2009;112(Suppl 1):S37–47.
[12] Schmidt M. Special issue: societal aspects of synthetic biology. Syst Synth Biol 2009;3(1–4):1–2.
[13] Kuzma J, Tanji T. Unpackaging synthetic biology: identification of oversight policy problems and options. Regul Governance 2010;4(1):92–112.
[14] Melchels FPW, Feijen J, Grijpma DW. A review on stereolithography and its applications in biomedical engineering. Biomaterials 2010;31(24):6121–30.
[15] Dimitrov D, Schreve K, De Beer N. Advances in three dimensional printing—state of the art and future perspectives. Rapid Prototyping J 2006;12 (3):136–47.
[16] Schubert C, Van Langeveld MC, Donoso LA. Innovations in 3D printing: a 3D overview from optics to organs. Br J Ophthalmol 2014;98(2):159–61.
[17] Ventola CL. Medical applications for 3D printing: current and projected uses. PT 2014;39(10):704–11.
[18] Gambello MJ, Iglewski BH. Cloning and characterization of the *Pseudomonas aeruginosa lasR* gene, a transcriptional activator of elastase expression. J Bacteriol 1991;173(9):3000–9.
[19] Kiratisin P, Tucker KD, Passador L. LasR, a transcriptional activator of *Pseudomonas aeruginosa* virulence genes, functions as a multimer. J Bacteriol 2002;184(17):4912–9.
[20] Schwarzer C, Fu Z, Fischer H, Machen TE. Redox-independent activation of NF-κB by *Pseudomonas aeruginosa* pyocyanin in a cystic fibrosis airway epithelial cell line. J Biol Chem 2008;283(40):27144–53.
[21] Pearson JP, Pesci EC, Iglewski BH. Roles of *Pseudomonas aeruginosa las* and *rhl* quorum-sensing systems in control of elastase and rhamnolipid biosynthesis genes. J Bacteriol 1997;179(18):5756–67.
[22] Seed PC, Passador L, Iglewski BH. Activation of the *Pseudomonas aeruginosa lasI* gene by LasR and the *Pseudomonas* autoinducer PAI: an autoinduction regulatory hierarchy. J Bacteriol 1995;177(3):654–9.
[23] Lyczak JB, Cannon CL, Pier GB. Lung infections associated with cystic fibrosis. Clin Microbiol Rev 2002;15(2):194–222.
[24] Maciá MD, Blanquer D, Togores B, Sauleda J, Pérez JL, Oliver A. Hypermutation is a key factor in development of multiple-antimicrobial resistance in *Pseudomonas aeruginosa* strains causing chronic lung infections. Antimicrob Agents Chemother 2005;49(8):3382–6.
[25] Pier GB, Grout M, Zaidi TS, Olsen JC, Johnson LG, Yankaskas JR, et al. Role of mutant CFTR in hypersusceptibility of cystic fibrosis patients to lung infections. Science 1996;271(5245):64–7.
[26] Pedersen SS, Espersen F, Høiby N. Diagnosis of chronic *Pseudomonas aeruginosa* infection in cystic fibrosis by enzyme-linked immunosorbent assay. J Clin Microbiol 1987;25(10):1830–6.
[27] McCulloch E, Lucas C, Ramage G, Williams C. Improved early diagnosis of *Pseudomonas aeruginosa* by real-time PCR to prevent chronic colonisation in a paediatric cystic fibrosis population. J Cyst Fibros 2011;10(1):21–4.
[28] Pearson JP, Gray KM, Passador L, Tucker KD, Eberhard A, Iglewski BH, et al. Structure of the autoinducer required for expression of *Pseudomonas aeruginosa* virulence genes. Proc Natl Acad Sci USA 1994;91(1):197–201.
[29] Maniatis T, Fritsch EF, Sambrook J. Molecular cloning: a laboratory manual. 2nd ed. New York: Cold Spring Harbor Laboratory Press; 1989.
[30] Ausubel FM, Brent R, Kingston R, Moore DD, Seidman J, Struhl K, et al. Current protocols in molecular biology. New York: John Wiley & Sons; 1987.
[31] Brophy JA, Voigt CA. Principles of genetic circuit design. Nat Methods 2014;11 (5):508–20.
[32] Hindmarsh AC. LSODE and LSODI, two new initial value ordinary differential equation solvers. ACM-SIGNUM Newslett 1980;15(4):10–1.
[33] COMSOL. COMSOL multiphysics: user's guide (version 4.3 a). Stockholm: COMSOL; 2012.
[34] Szykiedans K, Credo W. Mechanical properties of FDM and SLA low-cost 3-D prints. Procedia Eng 2016;136:257–62.
[35] Pardee K, Green AA, Ferrante T, Cameron DE, DaleyKeyser A, Yin P, et al. Paper-based synthetic gene networks. Cell 2014;159(4):940–54.
[36] Dubin PJ, Kolls JK. IL-23 mediates inflammatory responses to mucoid *Pseudomonas aeruginosa* lung infection in mice. Am J Physiol Lung Cell Mol Physiol 2007;292(2):L519–28.
[37] Jensen T, Pedersen SS, Garne S, Heilmann C, Høiby N, Koch C. Colistin inhalation therapy in cystic fibrosis patients with chronic *Pseudomonas aeruginosa* lung infection. J Antimicrob Chemother 1987;19(6):831–8.
[38] Ciofu O, Riis B, Pressler T, Poulsen HE, Høiby N. Occurrence of hypermutable *Pseudomonas aeruginosa* in cystic fibrosis patients is associated with the oxidative stress caused by chronic lung inflammation. Antimicrob Agents Chemother 2005;49(6):2276–82.
[39] Heeckeren A, Walenga R, Konstan MW, Bonfield T, Davis PB, Ferkol T. Excessive inflammatory response of cystic fibrosis mice to bronchopulmonary infection with *Pseudomonas aeruginosa*. J Clin Invest 1997;100(11):2810–5.
[40] Jahoor A, Patel R, Bryan A, Do C, Krier J, Watters C, et al. Peroxisome proliferator-activated receptors mediate host cell proinflammatory responses to *Pseudomonas aeruginosa* autoinducer. J Bacteriol 2008;190(13):4408–15.
[41] Kruger NJ. The Bradford method for protein quantitation. In: Walker JM, editor. Basic protein and peptide protocols. New York: Humana Press; 1994. p. 9–15.
[42] Swanson AB, Matev IB, de Groot G. The strength of the hand. Bull Prosthet Res 1970;10(14):145–53.